Probing quantum criticality with scanning tunneling spectroscopy

Minh-Tien Tran[1,2] and Ki-Seok Kim[1]
[1]*Asia Pacific Center for Theoretical Physics, POSTECH, Pohang, Gyeongbuk 790-784, Republic of Korea*
[2]*Institute of Physics, Vietnamese Academy of Science and Technology, P.O. Box 429, 10000 Hanoi, Vietnam*
(Received 7 October 2009; revised manuscript received 27 December 2009; published 28 January 2010)

We investigate the role of quantum coherence in tunneling conductance, where quantum criticality turns out to suppress Fano resonance. Based on the nonequilibrium noncrossing approximation, we show that the linear tunneling conductance exhibits weak Fano line shape with sharp cusp at zero energy in the multichannel Kondo effect resulting from incoherence associated with quantum criticality of impurity dynamics. In particular, shift of the peak position in the Fano resonance is predicted not to occur for the multichannel Kondo effect distinguished from the Fermi-liquid theory in the single-channel Kondo effect.

DOI: 10.1103/PhysRevB.81.035121 PACS number(s): 71.10.Hf, 68.37.Ef, 75.20.Hr, 75.30.Mb

I. INTRODUCTION

Recently, scanning tunneling microscopy (STM) has been utilized extensively to probe the electronic structure of materials with atomic scale spatial resolution. It was found that formation of the Kondo resonance gives rise to an asymmetric line shape in the tunneling conductance through the STM tip close to a magnetic adatom on a metallic surface,[1–3] the origin of which is an effect of interference between the direct tip-host tunneling and indirect tip-adatom-host one that resembles the so-called Fano resonance.[4] This Fano-Kondo effect has been discussed in detail.[5–7] A similar Fano-Kondo effect was also investigated in the electron transport through a quantum dot embedded in a closed Aharonov-Bohm interferometer.[8,9]

The mechanism of Fano resonance implies that quantum coherence of impurity dynamics plays an important role for the line shape, where the coherence time scale is estimated as $\sim 1/T_K$ with the Kondo temperature T_K. An interesting question is what happens in the Fano line shape if impurity dynamics becomes incoherent. Such a situation is realized in the multichannel Kondo system, where screening of a local moment by conduction electrons is overcompensated to drive the local Fermi-liquid state into a non-Fermi-liquid critical state first suggested by Nozieres and Blandin in the multichannel Kondo model.[10]

Multichannel Kondo impurity systems have been studied both experimentally and theoretically with considerable interests. Recently, the multichannel Kondo model was realized artificially in quantum dots.[11] The multichannel Kondo effect was also claimed to occur in the quadrupolar Kondo effect[12] and in metal point contacts.[13] In the theoretical respect the multichannel Kondo model has been studied in a variety of controlled techniques.[14] The conformal field theory approach provides exact results of the non-Fermi-liquid fixed point,[15] and the noncrossing approximation (NCA), exact in the limit of large number of spin flavors and charge channels, also gives practically sensible results,[16,17] where universal power-law scaling is found in physical responses. Such power-law physics distinguishes the critical non-Fermi-liquid state of the multichannel Kondo impurity from the local Fermi-liquid state of the single-channel Kondo impurity.

In this paper we study the Fano-Kondo effect by the tunneling current which flows from a single-channel STM tip to a multichannel Kondo impurity host. Instead of the standard Fano-Kondo resonance in the tunneling conductance, one may expect different pronounced features due to interference between the Fano resonance of the tunneling current and the overcompensated screening of an impurity. Employing the Keldysh nonequilibrium formalism,[18,19] we derive the tunneling current and its conductance, where the tunneling current solely depends on the Green's function of an impurity. We calculate the linear conductance profile analytically at zero temperature based on the nonequilibrium NCA (Refs. 20 and 21) to obtain nonequilibrium Green's functions of the impurity. A power-law line shape in the tunneling conductance clearly shows the overscreening effect of an impurity. Such an effect of incoherence leads the Fano resonance suppressed and its asymmetric feature becomes considerably weak. First of all, shift of the peak position in the Fano resonance turns out not to occur in the multichannel Kondo effect. These features are argued to be quite general distinguishing the non-Fermi-liquid phase from the Fermi-liquid state in STM.

The plan of the present paper is as follows. In Sec. II we present our model on an STM setup and derivation for the tunneling current. We introduce the nonequilibrium NCA in Sec. III. The conductance profile is analyzed at zero temperature in Sec. IV. Finally, the conclusion is presented in Sec. V.

II. TUNNELING CONDUCTANCE

A. Model

The system under consideration is shown schematically in Fig. 1. It consists of a multichannel Kondo impurity host and a single-channel STM tip placed directly above the host surface. The multichannel Kondo impurity host is modeled by a multichannel Anderson model in the slave-boson representation, which explicitly separates spin and channel excitations.[16] The STM tip couples separately to the impurity and to the local conduction electrons of the host.

The Hamiltonian of the system takes the form

$$H = H_{\text{host}} + H_{\text{tip}} + H_{\text{tunn}}, \tag{1}$$

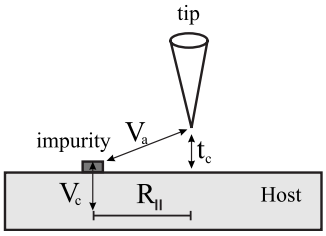

FIG. 1. Scanning tunneling microscope (STM) device with a tip placed closely to a Kondo impurity on the surface of a normal metal (host). In the host the impurity is hybridized with the metal conduction band through coupling V_c. The STM tip couples to the impurity via hopping V_a and to the local conduction electrons of the host via hopping t_c.

$$H_{\text{host}} = \sum_{\mathbf{k},\sigma,\tau} \varepsilon_{\mathbf{k}} c^{\dagger}_{\mathbf{k}\sigma\tau} c_{\mathbf{k}\sigma\tau} + \varepsilon_f \sum_{\sigma} f^{\dagger}_{\sigma} f_{\sigma} + V_c \sum_{\mathbf{k},\sigma,\tau} f^{\dagger}_{\sigma} b_{\bar{\tau}} c_{\mathbf{k}\sigma\tau} + \text{H.c.}, \tag{2}$$

$$H_{\text{tip}} = \sum_{\mathbf{k},\sigma} (E_{\mathbf{k}} - eV) a^{\dagger}_{\mathbf{k}\sigma} a_{\mathbf{k}\sigma}, \tag{3}$$

$$H_{\text{tunn}} = \sum_{\mathbf{k},\sigma,\tau} V_a(\mathbf{R}_t) f^{\dagger}_{\sigma} b_{\bar{\tau}} a_{\mathbf{k}\sigma} + \text{H.c.} + \sum_{\mathbf{k},\mathbf{p},\sigma,\tau} t_c(\mathbf{k},\mathbf{R}_{\|}) c^{\dagger}_{\mathbf{k}\sigma\tau} a_{\mathbf{p}\sigma} + \text{H.c.}, \tag{4}$$

where $c^{\dagger}_{\mathbf{k}\sigma\tau}$ ($a_{\mathbf{k}\sigma}$) creates host (tip) conduction electrons with wave vector $\mathbf{k}$, spin σ, and channel τ. The spin degeneracy is N and the number of channels is M. In the slave-boson representation the impurity creation operator is given by $f^{\dagger}_{\sigma} b_{\bar{\tau}}$, where f_{σ} is a fermion operator and $b_{\bar{\tau}}$ is a boson operator. The fermion, $f^{\dagger}_{\sigma}$, transforms according to $SU(N)$ and creates a local spin excitation, whereas the boson $b_{\bar{\tau}}$ transforms according to the conjugate representation of $SU(M)$ and annihilates the channel quantum number of the "vacuum" state produced by destroying a conduction electron.[16,17] Completeness of local states at the impurity site is represented by the constraint $\Sigma_{\sigma} f^{\dagger}_{\sigma} f_{\sigma} + \Sigma_{\bar{\tau}} b^{\dagger}_{\bar{\tau}} b_{\bar{\tau}} = 1$ implemented as usual by introducing a Lagrange multiplier λ. $\varepsilon_{\mathbf{k}}$ is the band dispersion of conduction electrons in the host and ε_f is the energy level of the Kondo impurity or the adatom at the host surface. V_c is the hybridization parameter of the impurity and conduction electrons in the host. For simplicity, V_c is assumed to be constant. $E_{\mathbf{k}}$ is the band dispersion of tip-conduction electrons and eV is an applied voltage bias between the tip and host, which causes a weak electron current to flow between them. We set the chemical potential of host conduction electrons as our reference energy.

Couplings between the impurity and tip-conduction electrons are represented by the hybridization parameter $V_a(\mathbf{R}_t)$, where $\mathbf{R}_t$ is the tip position. It decays with a tip-to-impurity separation[7]

$$V_a(\mathbf{R}_t) \approx V_a e^{-\kappa |R_t|},$$

where κ is an effective decay constant evaluated for states at the Fermi level of the tip. In this paper we consider $|R_t| \ll 1/\kappa$, thus, $V_a(\mathbf{R}_t)$ is modeled as a constant. Couplings between the tip and host conduction electrons are represented by $t_c(\mathbf{k},\mathbf{R}_{\|})$, where $\mathbf{R}_{\|}$ is a parallel distance between the tip and impurity. For plane waves of conduction electrons, we have

$$t_c(\mathbf{k},\mathbf{R}_{\|}) = t_c e^{-i\mathbf{k}\mathbf{R}_{\|}}.$$

When the tip is placed directly on top of the impurity, we take $t(\mathbf{k},\mathbf{R}_{\|}) = t_c$.

The host Hamiltonian of Eq. (2) is the multichannel Anderson model. In the case of $M=N$ the impurity is completely screened to form the Kondo singlet resulting in the local Fermi liquid. When the number of channels is larger than the spin degeneracy ($M>N$), the impurity is overcompensated to give rise to a non-Fermi-liquid fixed point, which exhibits universal power-law scaling.[15–17] The universal scaling property lies at the heart of quantum critical phenomena in a number of materials. In this respect the present study can be said to probe non-Fermi-liquid physics with STM. Unfortunately, experimental realization of the multichannel Anderson model is still problematic. Recently, the two-channel Kondo effect was realized artificially in quantum dots.[11] If the STM tip is applied to one of the leads, such non-Fermi-liquid physics would be observed.

B. Tunneling current

The electron current flowing between the tip and host is calculated within the Keldysh nonequilibrium formalism.[18,19] The current from the tip to the host is given by the time evolution of the occupation number for the electrons in the tip

$$J_{t\to h}(t) = e\left\langle \frac{dN_t}{dt} \right\rangle = -\frac{ie}{\hbar}\langle [H(t), N_t(t)] \rangle, \tag{5}$$

where $N_t = \Sigma_{\mathbf{k}\sigma} a^{\dagger}_{\mathbf{k}\sigma} a_{\mathbf{k}\sigma}$. One can express the current via nonequilibrium Green's functions

$$J_{t\to h}(t) = \frac{e}{\hbar} \sum_{\mathbf{k},\sigma,\tau} V^{*}_a G^{<}_{d\sigma\tau,a\mathbf{k}\sigma}(t,t) + \frac{e}{\hbar} \sum_{\mathbf{k},\mathbf{p},\sigma,\tau} t^{*}_c G^{<}_{c\mathbf{p}\sigma\tau,a\mathbf{k}\sigma}(t,t) + \text{H.c.}, \tag{6}$$

where

$$G^{<}_{d\sigma\tau,a\mathbf{k}\sigma}(t,t') = i\langle a^{\dagger}_{\mathbf{k}\sigma}(t') d_{\sigma\tau}(t) \rangle, \tag{7}$$

$$G^{<}_{c\mathbf{p}\sigma\tau,a\mathbf{k}\sigma}(t,t') = i\langle a^{\dagger}_{\mathbf{k}\sigma}(t') c_{\mathbf{p}\sigma\tau}(t) \rangle \tag{8}$$

are lesser Green's functions. Here we use the notation $d_{\sigma\tau} = b^{\dagger}_{\bar{\tau}} f_{\sigma}$.

In the steady-state nonequilibrium Green's functions depend only on $t-t'$, and the Fourier transformation results in

$$J_{t\to h} = \frac{e}{\hbar}\sum_{\sigma,\tau}\int d\omega V_a^* G^<_{d\sigma\tau,a\sigma}(\omega) + \frac{e}{\hbar}\sum_{\sigma,\tau}\int d\omega t_c^* G^<_{c\sigma\tau,a\sigma}(\omega) + \text{H.c.}, \tag{9}$$

where $G^<_{d\sigma\tau,a\sigma}(\omega)$ and $G^<_{c\sigma\tau,a\sigma}(\omega)$ are the Fourier transformations of $\Sigma_{\mathbf{k}} G^<_{d\sigma\tau,a\mathbf{k}\sigma}(t,t')$, $\Sigma_{\mathbf{k},\mathbf{p}} G^<_{c\mathbf{p}\sigma\tau,a\mathbf{k}\sigma}(t,t')$, respectively. These nonequilibrium Green's functions can be expressed via the impurity Green's function based on the equation of motion method. Detailed calculations are presented in Appendix A.

In a similar way we can calculate a current flowing from the host to the tip

$$J_{h\to t}(t) = e\left\langle \frac{dN_c}{dt}\right\rangle = -\frac{ie}{\hbar}\langle [H(t),N_c(t)]\rangle \tag{10}$$

with $N_c = \Sigma_{\mathbf{k}\sigma\tau} c^\dagger_{\mathbf{k}\sigma\tau} c_{\mathbf{k}\sigma\tau}$, where its detailed expression is given by Eq. (A13) in Appendix A.

Calling $J_{h\to t} = -J_{t\to h}$ in the steady state, the steady current can be rewritten in the form

$$J = yJ_{t\to h} - (1-y)J_{h\to t}, \tag{11}$$

where y is an arbitrary number. We choose y such that the term associated with the lesser Green's function $G^<_{d\sigma\tau,d\sigma\tau}(\omega)$ vanishes in the current formula from Eqs. (A12) and (A13). As a result, the electron current flowing between the tip and the host reads

$$J = \frac{e}{\hbar}\sum_{\sigma\tau}\int \frac{d\omega}{2\pi} T_{\text{tr}}(\omega)[f_a(\omega) - f_c(\omega)], \tag{12}$$

where

$$T_{\text{tr}}(\omega) = T_0 + Q_R \,\text{Re}\, G^R_{d\sigma\tau,d\sigma\tau}(\omega) + Q_I \,\text{Im}\, G^R_{d\sigma\tau,d\sigma\tau}(\omega), \tag{13}$$

and $f_{a(c)}(\omega)$ is the Fermi-Dirac distribution function for tip (host) conduction electrons. T_0 and the coefficients $Q_{R(I)}$ are defined as

$$T_0 = \frac{4\gamma}{(1+M\gamma)^2},$$

$$Q_R = 8\frac{1-M\gamma}{(1+M\gamma)^3}\sqrt{\gamma\Gamma_a\Gamma_c},$$

$$\begin{aligned} Q_I = {} & \frac{4}{(1+M\gamma)^3}\frac{1}{\Gamma_s}(\Gamma_a+\gamma\Gamma_c)(\Gamma_c+M\gamma\Gamma_a) \\ & - \frac{4(1-M\gamma)}{(1+M\gamma)^4}\frac{1}{\Gamma_s}[(\Gamma_a-\gamma\Gamma_c)(M\gamma\Gamma_a \\ & + \Gamma_c\{(1+M\gamma)[\gamma(M-1)+1]-\gamma\}) \\ & + (\Gamma_a+\gamma\Gamma_c)(\Gamma_c-\gamma\Gamma_a)] \\ & - \frac{4(M-1)\gamma}{(1+M\gamma)^4}\frac{1}{\Gamma_s}(\Gamma_c+\gamma\Gamma_a)[2\Gamma_c+(M\gamma-1)\Gamma_a], \end{aligned}$$

where $\Gamma_s = \Gamma_a + \Gamma_c[\gamma(M-1)+1]$. $\Gamma_{a(c)} = |V_{a(c)}|^2\pi\rho_{a(c)}$ is the coupling strength between the impurity and tip (host) conduction electrons, and $\gamma = \pi^2|t_c|^2\rho_a\rho_c$ is a measure of the strength for the direct tunneling of conduction electrons between the tip and the host. $\rho_{a(c)}$ is the density of states for noninteracting tip (host) conduction electrons at the Fermi level.

The current formula in Eqs. (12) and (13) can be viewed as a generalization of the Landauer-Büttiker formula to the STM case,[24,25] where $T_{\text{tr}}(\omega)$ is the transmission probability of the electron tunneling. The first term T_0 of the transmission probability is the direct tunneling between the tip and host, whereas the rest describe both indirect tunneling of conduction electrons through the impurity and interference between the two ways of electron tunneling. For the single-channel case ($M=1$) the current formula in Eq. (12) is reduced to the well-known formula.[9] In this case one may expect $\gamma \ll 1$ due to weakness of the tip coupling, hence, Q_R never vanishes. For the multichannel case $\gamma = 1/M$ may happen when the channel number M is large. In this special case $Q_R = 0$ and interference contributions to the tunneling current vanish. When $\gamma = 0$, i.e., there is no direct tunneling between the tip and host, only the last term of the transmission probability in Eq. (13) appears, associated with the indirect tunneling of electrons between the tip and host through the impurity. This contribution is proportional to the density of states (DOS) of the impurity. In the Kondo regime the impurity is screened by conduction electrons of the host, and this many-body effect must reflect in the DOS of the impurity, hence, also in the tunneling current. In general, the transmission probability $T_{\text{tr}}(\omega)$ is a superposition of the continuous direct tunneling, indirect tunneling, and their interferences giving rise to the Fano resonance.[4]

C. Discussion

The linear conductance is given by

$$G(\omega) = \left.\frac{\partial J(\omega)}{\partial eV}\right|_{eV=0} = \frac{e}{h}\sum_{\sigma\tau} T_{\text{tr}}(\omega) \tag{14}$$

at zero temperature. In general, the presence of the STM tip could affect physical properties of the host with the Kondo impurity. We will discuss this point in Sec. IV C. However, if couplings of the tip to the host and impurity are weak, influences of the tip on the host and impurity are negligible, where the impurity Green's function can be evaluated without couplings of the tip.

The impurity Green's function can be written in the form of the Dyson equation

$$G^R_{d\sigma\tau,d\sigma\tau} = \frac{1}{\omega - \varepsilon_d + i\Gamma_c - \Sigma(\omega)}, \tag{15}$$

where $\Sigma(\omega)$ is the retarded self-energy of the impurity Green's function. Considering real and imaginary parts of the retarded self-energy, $\Sigma(\omega) = \Sigma_R(\omega) - i\Sigma_I(\omega)$, we obtain the conductance profile in the form of

$$T_{\text{tr}}(\omega) = T_0\frac{[\Omega(\omega)+q(\omega)]^2 + p(\omega)}{\Omega^2(\omega)+1}, \tag{16}$$

where

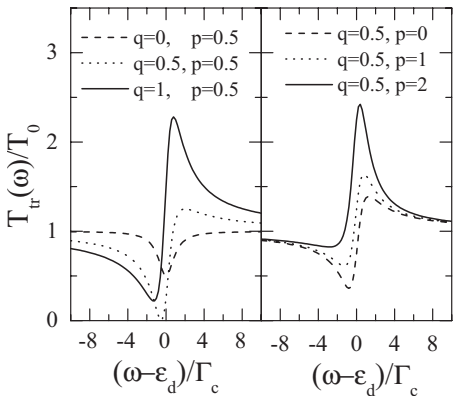

FIG. 2. Conductance profile in the noninteraction case for various parameters q and p as indicated in the figure.

$$\Omega(\omega) = \frac{\omega - \varepsilon_d - \Sigma_R(\omega)}{\Gamma_c + \Sigma_I(\omega)},$$

$$q(\omega) = \frac{(1+M\gamma)^2}{8\gamma}\frac{Q_R}{\Gamma_c + \Sigma_I(\omega)},$$

$$p(\omega) = 1 - q^2(\omega) - \frac{(1+M\gamma)^2}{4\gamma}\frac{Q_I}{\Gamma_c + \Sigma_I(\omega)}.$$

In the large frequency limit $\Sigma_R(\omega) \to$ const and $\Sigma_I(\omega) \to 0$ result, thus, we have $T_{\rm tr}(\omega) \to T_0$, nothing but the background profile of the conductance given by the direct tunneling probability between the tip and host.

The conductance profile in Eq. (16) can be viewed as a generalized Fano form. In the noninteraction case of $\Sigma(\omega) = 0$ we have $\Omega(\omega) = (\omega - \varepsilon_d)/\Gamma_c$, and $p(\omega)$ and $q(\omega)$ are constants. In this case the Fano resonance results from the interference effect of a Lorentzian line shape of a discrete level with a flat continuous background. The quantity q is the so-called asymmetry parameter of the Fano line shape, whereas the quantity p shifts positions of the maximum and minimum in the Fano line shape. In Fig. 2 we present the conductance profile for various parameters of q and p. It shows the Fano-resonance line shape like the Lorentzian one, the width of which is of order of Γ_c. For $q=0$ the profile line shape is symmetric and its asymmetry becomes obvious as q increases. The parameter p not only affects the maximum and minimum positions of the Fano line shape, but also makes the line-shape asymmetry clearer. One can expect that when interactions are included, the conductance profile will be significantly modified by the impurity self-energy as well as the Fano resonance.

III. NONEQUILIBRIUM NONCROSSING APPROXIMATION

The impurity Green's function is evaluated within the nonequilibrium NCA derived in a similar way as the equilibrium case.[17] We start from an Anderson model in the slave-boson representation

$$\begin{aligned} S_{\rm eff} = & \int\int dt dt' \sum_{\sigma\tau} c^\dagger_{\sigma\tau}(t)[G^0_{c\sigma\tau,c\sigma\tau}(t,t')]^{-1} c_{\sigma\tau}(t') \\ & + \int dt \sum_\sigma f^\dagger_\sigma(t)(i\partial_t - \varepsilon_d - i\lambda) f_\sigma(t) \\ & + \int dt \sum_\tau b^\dagger_{\bar\tau}(t)(i\partial_t - i\lambda) b_{\bar\tau}(t) + \int dt i\lambda \\ & + \int dt V_c f^\dagger_\sigma(t) b_{\bar\tau}(t) c_{\sigma\tau}(t) + \text{H.c.}, \end{aligned} \tag{17}$$

where $G^0_{c\sigma\tau,c\sigma\tau}(t,t')$ is the nonequilibrium single-site noninteracting Green's function for host conduction electrons and time integration is performed along the Keldysh time contour.

Integrating over conduction electron fields and introducing two bilocal fields $\Sigma_f(t,t')$ and $\Sigma_b(t,t')$ conjugate to $\Sigma_\sigma f^\dagger_\sigma(t) f_\sigma(t')$ and $\Sigma_\tau b^\dagger_{\bar\tau}(t) b_{\bar\tau}(t')$, respectively, the quartic term in the effective action can be decoupled as follows:

$$\begin{aligned} S_{\rm eff} = & \int dt \sum_\sigma f^\dagger_\sigma(t)(i\partial_t - \varepsilon_d - i\lambda) f_\sigma(t) \\ & + \int dt \sum_\tau b^\dagger_{\bar\tau}(t)(i\partial_t - i\lambda) b_{\bar\tau}(t) \\ & + \int dt i\lambda - \int\int dt dt' \Sigma_f(t',t) \sum_\tau b^\dagger_{\bar\tau}(t') b_{\bar\tau}(t) \\ & - \int\int dt dt' \Sigma_b(t,t') \sum_\sigma f^\dagger_\sigma(t) f_\sigma(t') \\ & - \int\int dt dt' \Sigma_b(t,t') D_0^{-1}(t,t') \Sigma_f(t',t), \end{aligned} \tag{18}$$

where $D_0(t,t') = |V_c|^2 G^0_{c\sigma\tau,c\sigma\tau}(t,t')$ is the hybridization function.

The nonequilibrium NCA is the saddle-point approximation of the effective Keldysh action for the bilocal fields $\Sigma_f(t,t')$ and $\Sigma_b(t,t')$. Introducing nonequilibrium fermionic and bosonic Green's functions as $F(t,t') = -i\langle T_c f_\sigma(t) f^\dagger_\sigma(t')\rangle$ and $B(t,t') = i\langle T_c b_{\bar\tau}(t) b^\dagger_{\bar\tau}(t')\rangle$, we find the saddle-point equations for the fermionic and bosonic self-energies

$$\Sigma_f(t,t') = iMD_0(t,t')B(t,t'), \tag{19}$$

$$\Sigma_b(t,t') = -iND_0(t',t)F(t,t'), \tag{20}$$

where the bilocal fields play the role of self-energies of the fermionic and bosonic Green's functions in the saddle-point approximation given by

$$F^{-1}(t,t') = \delta(t,t')(i\partial_t - \varepsilon_d - i\lambda) - \Sigma_f(t,t'), \tag{21}$$

$$B^{-1}(t,t') = \delta(t,t')(i\partial_t - i\lambda) - \Sigma_b(t,t'). \tag{22}$$

Variation in the effective action with respect to the Lagrange multiplier λ gives rise to the constraint equation

$$N\langle f^\dagger_\sigma f_\sigma\rangle + M\langle b^\dagger_{\bar\tau} b_{\bar\tau}\rangle = 1. \tag{23}$$

Using the Langreth's rule of analytical continuation on the real time axis,[22,23] self-energy equations (19) and (20) are

$$\Sigma_f^R(t,t') = iM\{[D_0^R(t,t') + D_0^<(t,t')]B^R(t,t') + D_0^R(t,t')B^<(t,t')\}, \tag{24}$$

$$\Sigma_b^R(t,t') = -iN[D_0^<(t',t)F^R(t,t') + D_0^A(t',t)F^<(t,t')], \tag{25}$$

$$\Sigma_f^<(t,t') = iMD_0^<(t,t')B^<(t,t'), \tag{26}$$

$$\Sigma_b^<(t,t') = -iND_0^>(t',t)F^<(t,t'). \tag{27}$$

In the steady state the Fourier transformation for the Green's functions and their self-energies results in the following nonequilibrium NCA equations:

$$\Sigma_f^R(\omega) = M\Gamma_c\int\frac{d\varepsilon}{2\pi}B^<(\varepsilon) + M\Gamma_c\int\frac{d\varepsilon}{\pi}f_c(\varepsilon-\omega)B^R(\varepsilon), \tag{28}$$

$$\Sigma_b^R(\omega) = N\Gamma_c\int\frac{d\varepsilon}{2\pi}F^<(\varepsilon) + N\Gamma_c\int\frac{d\varepsilon}{\pi}f_c(\varepsilon-\omega)F^R(\varepsilon), \tag{29}$$

$$\Sigma_f^<(\omega) = -M\int\frac{d\varepsilon}{\pi}f_c(\omega-\varepsilon)B^<(\varepsilon), \tag{30}$$

$$\Sigma_b^<(\omega) = -N\int\frac{d\varepsilon}{\pi}f_c(\omega-\varepsilon)F^<(\varepsilon), \tag{31}$$

where we have used explicit expressions for the hybridization function

$$D_0^R(\omega) = |V_c|^2G^{0R}_{c\sigma\tau,c\sigma\tau}(\omega) = -i\Gamma_c, \tag{32}$$

$$D_0^<(\omega) = |V_c|^2G^{0<}_{c\sigma\tau,c\sigma\tau}(\omega) = 2i\Gamma_c f_c(\omega). \tag{33}$$

Note that the first terms in Eqs. (28) and (29) are just constants. They can be absorbed into the Lagrange multiplier using the constraint Eq. (23) and

$$\langle f_\sigma^\dagger f_\sigma\rangle = -i\int\frac{d\varepsilon}{2\pi}F^<(\varepsilon), \tag{34}$$

$$\langle b_\tau^\dagger b_\tau\rangle = i\int\frac{d\varepsilon}{2\pi}B^<(\varepsilon). \tag{35}$$

We also used the fact that the Lagrange multiplier takes a large value at the end of calculations.[20,21]

Dyson equations (21) and (22) can be also rewritten for the retarded and lesser Green's functions based on the Langreth's rule of analytical continuation,

$$F^R(\omega) = \frac{1}{\omega-\varepsilon_d-i\lambda-\Sigma_f^R(\omega)}, \tag{36}$$

$$B^R(\omega) = \frac{1}{\omega-i\lambda-\Sigma_b^R(\omega)}, \tag{37}$$

$$F^<(\omega) = F^R(\omega)\Sigma_f^<(\omega)F^A(\omega), \tag{38}$$

$$B^<(\omega) = B^R(\omega)\Sigma_b^<(\omega)B^A(\omega). \tag{39}$$

Finally, the impurity Green's function can be calculated via the fermionic and bosonic Green's functions

$$G^R_{d\sigma\tau,d\sigma\tau}(\omega) = i\int\frac{d\varepsilon}{2\pi}[F^<(\omega+\varepsilon)B^A(\varepsilon) + F^R(\omega+\varepsilon)B^<(\varepsilon)]. \tag{40}$$

Inserting this impurity Green's function into the transmission coefficient, we find the conductance profile measured in STM.

The present derivation of nonequilibrium NCA equations can be viewed as the path integral version for the projection method[20,21] completely equivalent with each other. In practice, such NCA equations are first solved for retarded Green's functions, and lesser Green's functions are found with the use of the retarded Green's functions. In the next section we will perform this work.

IV. FANO RESONANCE IN THE MULTICHANNEL KONDO EFFECT

A. Zero-temperature solution of the noncrossing approximation equations

In the linear-response regime the host-electron distribution function $f_c(\omega)$ is given by the standard Fermi-Dirac distribution function. Then, NCA equations (28) and (29) for the retarded Green's functions resemble the equilibrium NCA equations solved exactly at zero temperature.[26,27] Equations (28) and (29) can be written as the following differential equations at zero temperature:

$$\frac{d\Sigma_f^R(\omega)}{d\omega} = \frac{M\Gamma_c}{\pi}B^R(\omega), \tag{41}$$

$$\frac{d\Sigma_b^R(\omega)}{d\omega} = \frac{N\Gamma_c}{\pi}F^R(\omega), \tag{42}$$

with the boundary condition $\Sigma_f^R(-D)=\Sigma_b^R(-D)=0$, where D is the band cutoff.

Solving these NCA equations, one can find

$$-[F^R(\omega)]^{-1} = T_K h_{N/M}\left[\frac{E_0-\omega}{T_K}, \frac{T_K}{\Gamma_c}\right], \tag{43}$$

where the scaling function $h_\alpha[x]$ is given by

$$x = \int_0^{h_\alpha[x,c]} dy\frac{W[y^\alpha e^{\pi\alpha c y}]}{1+W[y^\alpha e^{\pi\alpha c y}]}. \tag{44}$$

$W[x]$ is the Lambert W function defined as[28]

$$x = W[x]\exp(W[x]).$$

$T_K = D[M\Gamma_c/\pi D]^{M/N}\exp[\pi\varepsilon_d/N\Gamma_c]$ is identified with the Kondo energy scale, below which the multichannel Kondo

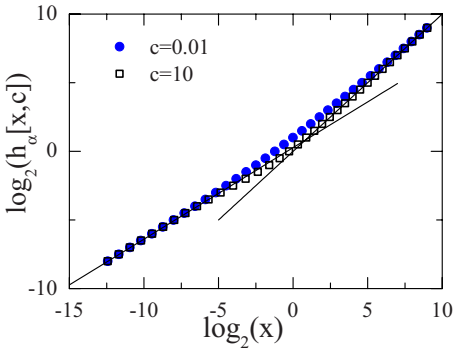

FIG. 3. (Color online) Scaling function $h_\alpha[x,c]$ with $\alpha=0.5$ and various parameters c. The two asymptotes $[(\alpha+1)x]^{1/(\alpha+1)}$ and x are shown as the solid lines.

effect arises. E_0 is the ground-state energy of the impurity, below which spectral densities of the fermionic and bosonic fields vanish at zero temperature.[26,27] Therefore, $F^R(\omega)$ and $B^R(\omega)$ are real functions below E_0. As shown in this expression, there are two energy scales Γ_c and T_K for the NCA solution. A detailed derivation can be found in Appendix B.

Equation (43) shows that the NCA solution obeys the universal scaling form. Although the scaling function in Eq. (44) should be computed numerically, its asymptotes in limits $x \ll 1$ and $x \gg 1$ can be found analytically. For $x \ll 1$, $W[x]=x-x^2$, thus, we obtain the asymptote

$$h_\alpha(x,c) = [(\alpha+1)x]^{1/(\alpha+1)}\left\{1 - \frac{\pi\alpha c}{\alpha+2}[(\alpha+1)x]^{1/(\alpha+1)} + \frac{2}{2\alpha+1}[(\alpha+1)x]^{\alpha/(\alpha+1)}\right\}. \quad (45)$$

The leading term of the scaling function $h_\alpha[x,c]$ shows the power scaling with an exponent $1/(\alpha+1)$ implying that both the retarded fermionic and bosonic Green's functions exhibit power-law physics near the threshold energy E_0. This corresponds to the overcompensated regime, where the impurity spin is overscreened by multichannel conduction electrons.[15–17] In the opposite limit $x \gg 1$, we obtain $h_\alpha[x,c]=x$ leading the fermionic Green's function to behave like $1/\omega$. This corresponds to the free moment regime, where the impurity spin is weakly bound to screening clouds.

In Fig. 3 we plot the scaling function $h_\alpha[x,c]$. This NCA solution [Eqs. (B6) and (43)] may be viewed as the complete solution of the NCA equations at zero temperature for all energy scales below the high-energy cutoff. It shows that the scaling function $h_\alpha[x,c]$ crosses from the power scaling regime to the linear behavior as x increases from zero. The scaling function $h_\alpha[x,c^*]$ obeys the power law up to $x \approx 1$, where c^* is identified with a "crossover" value. On the other hand, the power law of the scaling function is valid only for $x \ll 1$ when $c \ll c^*$. This property implies that there is a characteristic value of $(T_K/\Gamma_c)^*$ leading the power scaling to persist until energies comparable to T_K. In the conventional case of $T_K/\Gamma_c \ll 1$ the power scaling holds only for energies much below T_K. In the scaling regime $F^R(\omega) \sim (|\omega - E_0|/T_K)^{M/(N+M)}$ and $B^R(\omega) \sim (|\omega - E_0|/T_K)^{N/(N+M)}$ result obtained previously.[26,27] Although such power-law scaling fails to describe Fermi liquid in $T < T_K$ for the single-channel case, it is the underlying physics of the overcompensated screening impurity in the multichannel case as shown by the conformal field theory.[15]

The lesser self-energies obey the following differential equations:

$$\frac{d\Sigma_f^<(\omega)}{d\omega} = \frac{M\Gamma_c}{\pi}B^<(\omega), \quad (46)$$

$$\frac{d\Sigma_b^<(\omega)}{d\omega} = \frac{N\Gamma_c}{\pi}F^<(\omega) \quad (47)$$

at zero temperature. In the scaling regime the lesser Green's functions also display the same power scaling as the retarded ones given by[26,27]

$$F^<(\omega) = iA\frac{1}{Y_f(\omega)}, \quad (48)$$

$$B^<(\omega) = -iA\frac{1}{Y_b(\omega)}, \quad (49)$$

with $A=2\pi/(N+M)$. See Appendix B. Based on Eq. (43) with Eq. (B6) and Eqs. (48) and (49), we find the final expression for the impurity Green's function from Eq. (40) in the scaling regime,

$$G^R_{d\sigma\tau,d\sigma\tau}(\omega) = G^R_{d\sigma\tau,d\sigma\tau}(0) + \Delta G_{d\sigma\tau,d\sigma\tau}(\omega),$$

$$G^R_{d\sigma\tau,d\sigma\tau}(0) = \frac{1}{N+M}\frac{\pi}{\Gamma_c}\left[\frac{1}{M} - \frac{N+M}{N}n_f - \frac{\pi}{N+M}\cot\left(\frac{\pi M}{N+M}\right) - i\frac{\pi}{N+M}\right],$$

$$\Delta G_{d\sigma\tau,d\sigma\tau}(\omega) = i\frac{4\pi}{(N+M)\Gamma_c}\sin\left(\frac{\pi M}{N+M}\right) \times\left[\frac{M}{2N+M}B\left(\frac{2N}{N+M},\frac{M}{N+M}\right) \times\left(-\frac{N+M}{M}\frac{\omega}{T_K}\right)^{N/N+M} + \frac{\pi T_K}{(N+2M)\Gamma_c}B\left(\frac{N}{N+M},\frac{2M}{N+M}\right) \times\left(\frac{N+M}{M}\frac{\omega}{T_K}\right)^{M/N+M}\right], \quad (50)$$

where $B(x,y)$ is the beta function,[29] and $n_f=\langle f_\sigma^\dagger f_\sigma\rangle$.

The impurity Green's function exhibits two power scalings with $N/(M+N)$ and $M/(N+M)$. In the overcompensation case $(M>N)$ the power $N/(N+M)$ scaling is dominant for $\omega < T_{\mathrm{NCA}}$, where T_{NCA} is the crossover energy when the dominant scaling behavior of the impurity Green's function crosses from one power to another given by

$$T_{\mathrm{NCA}} = T_K \frac{M}{N+M}\left[\frac{M(N+2M)\Gamma_c}{(2N+M)\pi T_K}\frac{B\left(\frac{2N}{N+M},\frac{M}{N+M}\right)}{B\left(\frac{N}{N+M},\frac{2M}{N+M}\right)}\cos\left(\frac{\pi M}{N+M}\right)\right]^{N+M/M-N}. \quad (51)$$

B. Conductance profile within the noncrossing approximation

The impurity Green's function Eq. (50) is nonanalytic at $\omega=0$ exhibiting an asymmetric and sharp cusp with power-law scaling around $\omega=0$. These non-Fermi-liquid features are reflected on the conductance profile in Eq. (16). For comparison, we also calculate the conductance profile in the Fermi-liquid phase given by the following self-energy:[30]

$$\Sigma_{\mathrm{FL}}(\omega) = -\Gamma_c\left[\frac{\omega}{T_K} + i\frac{1}{2}\left(\frac{\omega}{T_K}\right)^2\right]. \quad (52)$$

In Fig. 4 we plot conductance profiles in the symmetric case, i.e., $\varepsilon_d=-\mathrm{Re}\,\Sigma(0)$, within the NCA and Fermi-liquid theory for various values of γ. It shows that the conductance profile of the overcompensation multichannel Kondo model shows a sharp cusp with power-law scaling at $\omega=0$ as expected. This feature is completely distinguished from the Fermi-liquid theory result, where the conductance profile exhibits the narrow Fano-Kondo resonance, the width of which is on the order of T_K. Note that the frequency in the x axis is scaled with T_K in Fig. 4, which is much smaller than the energy scale Γ_c in the noninteraction case (Fig. 2).

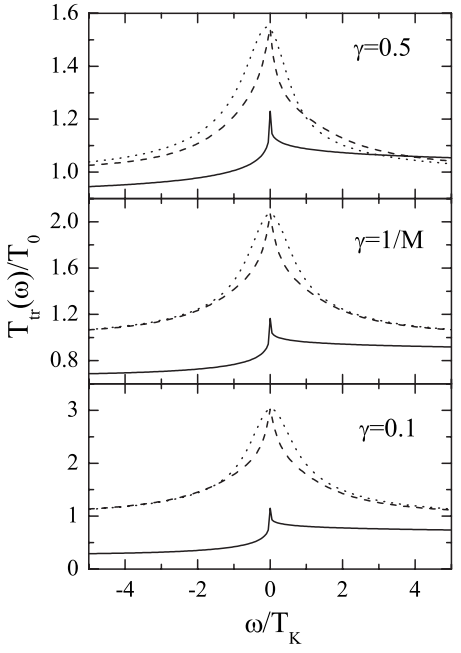

FIG. 4. Conductance profile calculated within the NCA (the solid lines), the marginal Fermi-liquid theory (the dashed lines), and the Fermi-liquid theory (the dotted lines) for various values of γ. Other parameters are $M=6$, $N=2$, $\Gamma_c=1$, $\Gamma_a=0.01$, $T_K=0.01$, and $n_f=0.8$.

In the case of $\gamma=1/M$ the asymmetry parameter $q(\omega)$ vanishes; thus, interference contributions to the conductance disappear. As we can see in Fig. 4, the Fermi-liquid conductance profile is symmetric and exhibits only the Kondo resonance at zero frequency. On the other hand, the asymmetry parameter $q(\omega)$ is finite for $\gamma\neq 1/M$, and the Fano resonance shifts the peak position away from zero, giving rise to an asymmetric feature in the conductance profile within the Fermi-liquid theory. Note that the asymmetry is more pronounced for larger γ.

In the multichannel case the conductance profile still exhibits an asymmetric feature even when $\gamma=1/M$. However, this asymmetry is not due to the Fano resonance but due to the non-Fermi-liquid feature in the density of states of the overscreened impurity. Although interference contributions to the conductance are finite for $\gamma\neq 1/M$, they cannot shift the peak position away from zero in the multichannel conductance as in the Fermi-liquid theory, the hallmark of non-Fermi-liquid physics measured in STM. The conductance profile still exhibits the sharp cusp at $\omega=0$. This asymmetry is due to both interference contributions and non-Fermi-liquid properties of the overscreened impurity. However, interference contributions are so weak that the Fano resonance is suppressed. This indicates dominance of the non-Fermi-liquid overcompensation over the Fano resonance. In the multichannel case the conductance profile shows weak dependence on γ, thus, the strength of the tip coupling is not essential to detect the non-Fermi-liquid feature in the tunneling conductance, as far as it does not vanish.

C. Physical origin for suppression of the Fano resonance

In the Fermi-liquid phase one can see $\Omega(\omega)\sim\omega$ and $q(\omega)$, $p(\omega)\sim$const as $\omega\to 0$ in the tunneling conductance [Eq. (16)] from Eq. (52), giving rise to the Fano resonance away from $\omega=0$. This originates from quantum coherence of impurity dynamics, which maintains $\Sigma_R(\omega)\sim\omega$ and $\Sigma_I(\omega)\sim\omega^2$ as $\omega\to 0$. In the multichannel overcompensation scaling regime $\Sigma_R(\omega)\sim\Sigma_I(\omega)\sim|\omega|^{N/(N+M)}$ results when $\omega\to 0$, which leads $\Omega(\omega)\sim 1$ and the asymmetry factor $q(\omega)\sim|\omega|^{-N/(N+M)}$, $p(\omega)\sim|\omega|^{-N/(N+M)}$. As a consequence we find $T_{\mathrm{tr}}(\omega)\sim|\omega|^{-2N/(N+M)}$ in $\omega\to 0$. The conductance profile always exhibits its peak at $\omega=0$ that indicates the peak position does not shift unlike the Fermi-liquid theory. This can be interpreted as the fact that quantum coherence of impurity dynamics is lost in the multichannel scaling regime, hence, suppressing the Fano resonance.

For comparison we also calculate the conductance profile in a marginal Fermi-liquid phase given by the following self-energy ansatz:[31]

$$\Sigma_{\mathrm{MFL}}(\omega) = \Gamma_c \left[\frac{\omega}{T_K} \log \frac{|\omega|}{T_K} - i \frac{\pi}{2} \frac{|\omega|}{T_K} \right]. \tag{53}$$

The marginal Fermi-liquid phase can be considered as an intermediate case which lies between the Fermi-liquid phase and multichannel overcompensation phase, where the impurity dynamics maintains weak quantum coherence. In Fig. 4 we also plot the conductance profile in the marginal Fermi-liquid phase for various values of γ. It shows that the conductance profile of the marginal Fermi-liquid theory exhibits a narrow resonance nearby $\omega=0$. It resembles the conductance profile of the Fermi-liquid theory except for the position of the Fano resonance which is very close to $\omega=0$. The weak quantum coherence in the marginal Fermi-liquid phase can maintain the Fano resonance; however, weakness of its quantum coherence cannot significantly shift the peak position of the Fano resonance away from zero in comparison with the Fermi-liquid phase. This feature implies the important role of quantum coherence of impurity dynamics in the mechanism of Fano resonance. When the impurity dynamics becomes incoherent, the Fano resonance is suppressed.

D. Effect of the tip-host and the tip-impurity coupling on the M-channel Kondo impurity system

As mentioned in Sec. II C, the impurity Green's function is evaluated without the tip coupling in the conductance profile of Eq. (16). In general, the presence of the tip could affect physical properties of the host with the Kondo impurity. In this subsection we discuss the effects of the tip-host and the tip-impurity coupling on the M-channel Kondo impurity system of the host and impurity. Although such tip couplings break the $SU(M)$ symmetry in principle, we argue that the overcompensation Kondo effect still occurs for weak tip-impurity couplings with finite tip-host couplings.

1. Effect of the tip-host coupling

First, we consider the effect of the tip-host coupling only, where the tip-impurity coupling is neglected. We take the following unitary transformation for conduction electron fields $c_{\mathbf{k}\sigma\tau}$ and bosonic fields b_τ:

$$c_{\mathbf{k}\sigma\tau} = \sum_{\tau'} \mathbf{U}_{\tau\tau'} \tilde{c}_{\mathbf{k}\sigma\tau'}, \tag{54}$$

$$b_\tau = \sum_{\tau'} \mathbf{U}^\dagger_{\tau\tau'} \tilde{b}_{\tau'}, \tag{55}$$

where the $M \times M$ unitary matrix $\mathbf{U}$ is chosen to satisfy $\tilde{c}_{\mathbf{k}\sigma 1} = \Sigma_\tau c_{\mathbf{k}\sigma\tau}/\sqrt{M}$ for diagonalization of the tip to host coupling term. We rewrite the starting Hamiltonian Eq. (1) in the above transformed basis and integrate over tip conduction-electron fields. Then, we find

$$\begin{aligned} S_{\mathrm{eff}} = & \int d\tau \sum_{\mathbf{k}\sigma\tau} \tilde{c}^\dagger_{\mathbf{k}\sigma\tau}(\tau)(\partial_\tau - \varepsilon_{\mathbf{k}}) \tilde{c}_{\mathbf{k}\sigma\tau}(\tau) \\ & + \sum_\sigma f^\dagger_\sigma(\tau)(\partial_\tau + \lambda - \varepsilon_f) f_\sigma(\tau) \\ & + \sum_\tau \tilde{b}^\dagger_\tau(\tau)(\partial_\tau + \lambda) \tilde{b}_\tau(\tau) + V_c \sum_{\mathbf{k}\sigma\tau} f^\dagger_\sigma(\tau) \tilde{b}_\tau(\tau) \tilde{c}_{\mathbf{k}\sigma\tau}(\tau) + \mathrm{H.c.} \\ & + \int d\tau d\tau' M |t_c|^2 \sum_{\mathbf{k}\mathbf{k}'\sigma} \tilde{c}^\dagger_{\mathbf{k}\sigma 1}(\tau) g_a(\tau - \tau') \tilde{c}_{\mathbf{k}'\sigma 1}(\tau'), \end{aligned}$$

where $g_a(\tau-\tau')$ is the local Green's function for tip electrons.

It is clear that the last term in the above effective action breaks the $SU(M)$ symmetry. Effectively, the conduction channel $\tilde{c}_{\mathbf{k}\sigma 1}$ has an additional contribution $\sim M|t_c|^2\rho_a$ to its normal dispersion, while other conduction channels have not. Integrating over conduction electrons, we obtain

$$\begin{aligned} S_{\mathrm{eff}} = & \int d\tau \sum_\sigma f^\dagger_\sigma(\tau)(\partial_\tau + \lambda - \varepsilon_f) f_\sigma(\tau) \\ & + \sum_\tau \tilde{b}^\dagger_\tau(\tau)(\partial_\tau + \lambda) \tilde{b}_\tau(\tau) + \int d\tau d\tau' |V_c|^2 \end{aligned} \tag{56}$$

$$\begin{aligned} & \sum_\sigma f^\dagger_\sigma(\tau) \tilde{b}_1(\tau) \left\{ \sum_{\mathbf{k}\mathbf{k}'} g^{c(1)}_{kk'}(\tau - \tau') \right\} \tilde{b}^\dagger_1(\tau') f_\sigma(\tau') \\ & + \int d\tau d\tau' |V_c|^2 \sum_{\sigma, \tau \neq 1} f^\dagger_\sigma(\tau) \tilde{b}_\tau(\tau) \\ & \times \left\{ \sum_{\mathbf{k}\mathbf{k}'} g^{c}_{kk'}(\tau - \tau') \right\} \tilde{b}^\dagger_\tau(\tau') f_\sigma(\tau'), \end{aligned} \tag{57}$$

where $[g^{c(1)}_{kk'}(\tau-\tau')]^{-1} = -(\partial_\tau - \varepsilon_{\mathbf{k}})\delta_{kk'} - M|t_c|^2 g_a(\tau-\tau')$ is the inverse of the electron propagator for the channel $\tau=1$ and $[g^{c}_{kk'}(\tau-\tau')]^{-1} = -(\partial_\tau - \varepsilon_{\mathbf{k}})\delta_{kk'}$ is that for other $M-1$ channels. This $SU(M)$ symmetry breaking gives rise to anisotropic hybridization couplings. In Appendix C we prove that $\Gamma^{(1)}_c = |V_c|^2 \Sigma_{\mathbf{k}\mathbf{k}'} |\mathrm{Im}\, g^{c(1)}_{kk'}(0)| \leq \Gamma_c$ always happens. This indicates that the channel $\tau=1$ couples to the impurity weaker than $(M-1)$ rest channels. As a consequence, the $(M-1)$ channel Kondo effect would occur. For large M, there is no difference in the physics of the overcompensated Kondo effect between $(M-1)$ channels and M channels.

2. Effect of the tip-impurity coupling

Now we consider the effect of the tip-impurity coupling only, where the tip-host coupling is neglected. As performed in the previous section, we take again the unitary transformation in Eqs. (54) and (55) for conduction electron fields $c_{\mathbf{k}\sigma\tau}$ and bosonic fields b_τ, but now the $M \times M$ unitary matrix $\mathbf{U}$ is chosen to satisfy $\tilde{b}_1 = \Sigma_\tau b_\tau/\sqrt{M}$ for diagonalization of the tip-to-impurity coupling term. Then, we find the following effective action:

$$S_{\text{eff}} = \int d\tau \sum_{\sigma} f_{\sigma}^{\dagger}(\tau)(\partial_{\tau} + \lambda - \varepsilon_f) f_{\sigma}(\tau) + \sum_{\tau} \tilde{b}_{\tau}^{\dagger}(\tau)(\partial_{\tau} + \lambda)\tilde{b}_{\tau}(\tau)$$
$$+ \int d\tau d\tau' \sum_{\sigma} f_{\sigma}^{\dagger}(\tau)\tilde{b}_1(\tau)[|V_c|^2 g_c(\tau - \tau')$$
$$+ M|V_a|^2 g_a(\tau - \tau')]\tilde{b}_1^{\dagger}(\tau') f_{\sigma}(\tau')$$
$$+ \int d\tau d\tau' |V_c|^2 \sum_{\sigma,\tau\neq 1} f_{\sigma}^{\dagger}(\tau)\tilde{b}_{\tau}(\tau) g_c(\tau - \tau')\tilde{b}_{\tau}^{\dagger}(\tau') f_{\sigma}(\tau'),$$

where $g_c(\tau) = \Sigma_{\mathbf{k},\mathbf{k}'} g^c_{kk'}(\tau)$. This effective action shows that the tip-impurity coupling breaks the $SU(M)$ symmetry. The effective hybridization coupling of the effective channel $\tau = 1$ is $\Gamma_c + M\Gamma_a$, and it is always larger than the effective hybridization coupling Γ_c of the $(M-1)$ rest channels. As a consequence, the single-channel Kondo effect would occur. In this case the system restores the Fermi-liquid behaviors. The NCA at zero temperature produces spurious non-Fermi-liquid features[26,27] and it is not adequate to describe the physical properties of the system. In the calculation of the conductance profile the Fermi-liquid self-energy in Eq. (52) must be used and the Fano-Kondo resonance could appear.

3. Effect of both the tip-host and tip-impurity couplings

The two previous sections show that the tip-host coupling allows the overcompensation Kondo effect, while the tip-impurity coupling drives the system away from the critical regime. Therefore, we are mainly interested in the case of a finite tip-host coupling and small tip-impurity coupling. As the case of finite tip-host couplings, we take the unitary transformation for conduction electron fields $c_{\mathbf{k}\sigma\tau}$ and bosonic fields b_{τ} in Eqs. (54) and (55) with $\tilde{c}_{\mathbf{k}\sigma 1} = \Sigma_{\tau} c_{\mathbf{k}\sigma\tau}/\sqrt{M}$. Proceeding in a similar way as the previous sections, we find the effective action

$$S_{\text{eff}} = \int d\tau \sum_{\sigma} f_{\sigma}^{\dagger}(\tau)(\partial_{\tau} + \lambda - \varepsilon_f) f_{\sigma}(\tau) + \sum_{\tau} \tilde{b}_{\tau}^{\dagger}(\tau)(\partial_{\tau} + \lambda)\tilde{b}_{\tau}(\tau) + \sum_{\sigma,\tau\neq 1} \int d\tau d\tau' |V_c|^2 f_{\sigma}^{\dagger}(\tau)\tilde{b}_{\tau}(\tau) g_c(\tau - \tau')\tilde{b}_{\tau}^{\dagger}(\tau') f_{\sigma}(\tau')$$
$$+ \sum_{\sigma} \int d\tau d\tau' \Big\{ |V_c|^2 f_{\sigma}^{\dagger}(\tau)\tilde{b}_1(\tau) g^{c(1)}(\tau - \tau')\tilde{b}_1^{\dagger}(\tau') f_{\sigma}(\tau')$$
$$+ f_{\sigma}^{\dagger}(\tau) b_0(\tau) \Big[M|V_a|^2 g_a(\tau - \tau') + M^2|V_a|^2|t_c|^2 \int d\tau_1 d\tau_2 g_a(\tau - \tau_1) g^{c(1)}(\tau_1 - \tau_2) g_a(\tau_2 - \tau') \Big] b_0^{\dagger}(\tau') f_{\sigma}(\tau')$$
$$+ M V_c V_a^* t_c f_{\sigma}^{\dagger}(\tau)\tilde{b}_1(\tau) \int d\tau_1 g^{c(1)}(\tau - \tau_1) g_a(\tau_1 - \tau') b_0^{\dagger}(\tau') f_{\sigma}(\tau')$$
$$+ M V_c^* V_a t_c^* f_{\sigma}^{\dagger}(\tau) b_0(\tau) \int d\tau_1 g_a(\tau - \tau_1) g^{c(1)}(\tau_1 - \tau')\tilde{b}_1^{\dagger}(\tau') f_{\sigma}(\tau') \Big\}, \quad (58)$$

where $g^{c(1)}(\tau) = \Sigma_{\mathbf{k},\mathbf{k}'} g^{c(1)}_{kk'}(\tau)$, and $b_0 = \Sigma_{\tau} b_{\tau}/\sqrt{M}$. In general, b_0 is not necessarily equal to $\tilde{b}_1$. We can rewrite $b_0 = \alpha_1 \tilde{b}_1 + \alpha_2 \hat{b}$, where $\hat{b}$ is a linear combination of $\tilde{b}_2, \ldots, \tilde{b}_M$. The coefficients α_1 and α_2 satisfy $|\alpha_1|^2 + |\alpha_2|^2 = 1$.

In the wide band limit of a constant density of states for conduction electrons in both the tip and host, the effective hybridization coupling terms of M channels in Eq. (58) can be rewritten schematically as follows:

$$f_{\sigma}^{\dagger}\tilde{b}_1(\Gamma_c^{(1)} + |\alpha_1|^2\Gamma_a^{(0)} + \alpha_1^*\Gamma_{ac} + \alpha_1\Gamma_{ac}^*)\tilde{b}_1^{\dagger} f_{\sigma} + f_{\sigma}^{\dagger}\hat{b}|\alpha_2|^2\Gamma_a^{(0)}\hat{b}^{\dagger} f_{\sigma}$$
$$+ f_{\sigma}^{\dagger}\tilde{b}_1\alpha_2^*\Gamma_{ac}\hat{b}^{\dagger} f_{\sigma} + f_{\sigma}^{\dagger}\hat{b}\alpha_2\Gamma_{ac}^*\tilde{b}_1^{\dagger} f_{\sigma} + \sum_{\tau\neq 1} f_{\sigma}^{\dagger}\tilde{b}_{\tau}\Gamma_c\tilde{b}_{\tau}^{\dagger} f_{\sigma}, \quad (59)$$

where

$$\Gamma_a^{(0)} = M|V_a|^2|\text{Im } g_a(0)| + M^2|V_a|^2|t_c|^2|\text{Im}[g_a(0)^2 g^{c(1)}(0)]|,$$

$$\Gamma_{ac} = M V_c V_a^* t_c |\text{Im}[g_a(0) g^{c(1)}(0)]|.$$

One can show that $\Gamma_c^{(1)} = \Gamma_c/(1 + M\gamma)$, $\Gamma_a^{(0)} = M\Gamma_a/(1 + M\gamma)$, and $|\Gamma_{ac}|^2 = M^2\Gamma_c\Gamma_a\gamma/(1 + M\gamma)^2$. The hybridization coupling of $(M-1)$ channels Γ_c is expected to dominate over those of the channels $\tilde{b}_1$ and $\hat{b}$ if the following conditions are satisfied:

$$\Gamma_c > \Gamma_c^{(1)} + \Gamma_a^{(0)} + 2|\Gamma_{ac}|, \quad (60)$$

$$\Gamma_c^{(1)} > \Gamma_a^{(0)}. \quad (61)$$

These conditions are equivalent to $\Gamma_c > M\Gamma_a$ and $\gamma\Gamma_c > (3 + \sqrt{8})\Gamma_a$. When the hybridization couplings of $(M-1)$ channels are relevant, the $(M-1)$ channel Kondo effect would occur. For large M, there is again no difference in the physics of the overcompensated Kondo effect between $(M-1)$ channels and M channels. However, we admit that this expectation does not have a firm ground because there exists com-

plex mixing between channels. In our opinion this problem should deserve further investigation.

Finally, we would like to mention that our demonstration is expected to apply to the quantum dot realization for the multichannel Kondo effect. If the STM tip lies in the lead, we would be in weak Γ_a. Then, the suppression of the Fano resonance is expected to observe.

V. CONCLUSION

In the present paper we predicted an interesting feature of non-Fermi-liquid physics for the multichannel Kondo model based on the STM experimental setting (Fig. 1). Non-Fermi-liquid physics often occurs at the quantum phase transition and presents challenges in both theoretical and experimental aspects, for instance, quantum criticality in heavy fermion materials.[32] Heavy fermion materials can be modeled by the Anderson lattice model. One heavy fermion quantum critical point in the Anderson lattice model was argued to be captured in the so-called dynamical mean-field theoretical framework, more concretely, the two impurity Anderson model with self-consistency, expected to result in essentially similar physics with the multichannel impurity model.[33] As the first step to understand non-Fermi-liquid physics within the STM detection, we employed the multichannel Anderson model for one source of the non-Fermi-liquid state.

We derived the Landauer-Büttiker formula for the tunneling current from the STM tip to the multichannel impurity host based on the Keldysh nonequilibrium formalism, where the tunneling current is given by only the impurity Green's function. Employing the nonequilibrium NCA, we showed that the impurity Green's function exhibits universal power-law scaling at low energies. As a consequence, the tunneling conductance turns out to exhibit weak asymmetry but rather sharp cusp at zero energy resulting from the power-law scaling of the impurity Green's function. The conventional Fano resonance in Fermi liquids was shown to be suppressed. The main prediction of our study is that the peak position in the Fano-Kondo resonance does not shift, even increasing the tip coupling constant, clearly distinguished from the Fermi-liquid theory. Quantum coherence of the impurity dynamics turns out to play an important role in the Fano mechanism.

ACKNOWLEDGMENTS

We would like to thank T. Takimoto for useful discussions. This work was supported by the National Research Foundation of Korea (NRF) grant funded by the Korea government (MEST) (Grant No. 2009-0074542). One of the authors (M.-T.) was also supported by the Vietnamese NAFOSTED.

APPENDIX A: DERIVATION OF TUNNELING CURRENT

In Appendix A we derive the tunneling current formula in Eqs. (12) and (13). The lesser Green's functions in Eq. (9) are given by off-diagonal components of nonequilibrium Green's functions defined on the Keldysh time contour which runs on the time axis from $-\infty$ to ∞ and goes back to $-\infty$,[18,19]

$$G^c_{d\sigma\tau,a\mathbf{k}\sigma}(t,t') = -i\langle T_c d_{\sigma\tau}(t) a^\dagger_{\mathbf{k}\sigma}(t')\rangle, \tag{A1}$$

$$G^c_{c\mathbf{p}\sigma\tau,a\mathbf{k}\sigma}(t,t') = -i\langle T_c c_{\mathbf{p}\sigma\tau}(t) a^\dagger_{\mathbf{k}\sigma}(t')\rangle, \tag{A2}$$

where T_c is the time ordering operator on the Keldysh time contour. Differentiating the nonequilibrium Green's functions with respect to t' and resorting to the Heisenberg equation of motion

$$\frac{da^\dagger_{\mathbf{k}\sigma}(t')}{dt'} = -\frac{i}{\hbar}[H(t'), a^\dagger_{\mathbf{k}\sigma}(t')],$$

we obtain the following equations:

$$G^c_{d\sigma\tau,a\mathbf{k}\sigma}(t,t') = \int dt_1 V_a G^c_{d\sigma\tau,d\sigma\tau}(t,t_1) g^c_{a\mathbf{k}}(t_1,t') + \sum_{\mathbf{p},\tau'} \int dt_1 t_c G^c_{d\sigma\tau,c\mathbf{p}\sigma\tau'}(t,t_1) g^c_{a\mathbf{k}}(t_1,t'), \tag{A3}$$

$$G^c_{d\sigma\tau,c\mathbf{p}\sigma\tau'}(t,t') = \delta_{\tau\tau'} \int dt_1 V_c G^c_{d\sigma\tau,d\sigma\tau}(t,t_1) g^c_{c\mathbf{p}}(t_1,t') + \sum_{\mathbf{k}} \int dt_1 t_c^* G^c_{d\sigma\tau,a\mathbf{k}\sigma}(t,t_1) g^c_{c\mathbf{p}}(t_1,t'), \tag{A4}$$

where $g^c_{a\mathbf{k}}(t,t')$ and $g^c_{c\mathbf{k}}(t,t')$ are the nonequilibrium Green's functions for the isolated noninteracting conduction electrons in the tip and host, respectively.

Inserting Eq. (A4) into Eq. (A3), we obtain

$$G^c_{d\sigma\tau,a\sigma}(t,t') = \int dt_1 V_a G^c_{d\sigma\tau,d\sigma\tau}(t,t_1) g^c_a(t_1,t') + \int dt_1 \int dt_2 t_c V_c G^c_{d\sigma\tau,d\sigma\tau}(t,t_1) g^c_c(t_1,t_2) g^c_a(t_2,t') + \int dt_1 \int dt_2 M|t_c|^2 G^c_{d\sigma\tau,a\sigma}(t,t_1) g^c_c(t_1,t_2) g^c_a(t_2,t'), \tag{A5}$$

where $g^c_{a(c)}(t,t') = \Sigma_{\mathbf{k}} g^c_{a(c)\mathbf{k}}(t,t')$. Using the Langreth's rule of analytical continuation on the real time axis,[22,23] we can obtain the retarded (advanced) and lesser (or greater) Green's functions from Eq. (A5),

$$G^{R/A}_{d\sigma\tau,a\sigma} = V_a G^{R/A}_{d\sigma\tau,d\sigma\tau} * g^{R/A}_a + t_c V_c G^{R/A}_{d\sigma\tau,d\sigma\tau} * g^{R/A}_c * g^{R/A}_a + M|t_c|^2 G^{R/A}_{d\sigma\tau,a\sigma} * g^{R/A}_c * g^{R/A}_a, \tag{A6}$$

$$G^<_{d\sigma\tau,a\sigma} = V_a (G^R_{d\sigma\tau,d\sigma\tau} * g^<_a + G^<_{d\sigma\tau,d\sigma\tau} * g^A_a) + t_c V_c (G^R_{d\sigma\tau,d\sigma\tau} * g^R_c * g^<_a + G^R_{d\sigma\tau,d\sigma\tau} * g^<_c * g^A_a + G^<_{d\sigma\tau,d\sigma\tau} * g^A_c * g^A_a) + M|t_c|^2 (G^R_{d\sigma\tau,a\sigma} * g^R_c * g^<_a + G^R_{d\sigma\tau,a\sigma} * g^<_c * g^A_a + G^<_{d\sigma\tau,a\sigma} * g^A_c * g^A_a), \tag{A7}$$

where the superscripts R, A, and $<$ denote the retarded, advanced, and lesser Green's functions, respectively. For sim-

plifying to write equations, we use the so-called $*$ notation defined as $A(t)*B(t')=\int dt_1 A(t,t_1)B(t_1,t')$.

In the steady state Eqs. (A6) and (A7) are easily solved making the Fourier transformation. As a result, we find

$$\begin{aligned} G^<_{d\sigma\tau,a\sigma}(\omega) = {} & G^R_{d\sigma\tau,d\sigma\tau}(\omega)Z^A(\omega)\{V_a g^<_a(\omega) + (t_c V_c + M|t_c|^2) \\ & \times[g^R_c(\omega)g^<_a(\omega) + g^<_c(\omega)g^A_a(\omega)]\} \\ & + G^<_{d\sigma\tau,d\sigma\tau}(\omega)Z^A(\omega)[V_a g^A_a(\omega) \\ & + t_c V_c g^A_c(\omega)g^A_a(\omega)], \end{aligned} \tag{A8}$$

where $Z^{R/A}(\omega)=1/[1-M|t_c|^2 g^{R/A}_c(\omega)g^{R/A}_a(\omega)]$.

Performing in a similar way, we can express the Green's function $G^c_{c\sigma,a\sigma}(t,t')=\Sigma_{\mathbf{k},\mathbf{p},\tau}G^c_{c\mathbf{k}\sigma\tau,a\mathbf{p}\sigma}(t,t')$ with $G^c_{d\sigma,a\sigma}(t,t')=\Sigma_\tau G^c_{d\sigma\tau,a\sigma}(t,t')$. One can verify

$$\begin{aligned} G^<_{c\sigma,a\sigma}(\omega) = {} & Mt_c Z^R(\omega)[g^R_c(\omega)g^<_a(\omega) + g^<_a(\omega)g^A_a(\omega)][1 \\ & + M|t_c|^2 Z^A(\omega)g^A_c(\omega)g^A_a(\omega)] + G^<_{d\sigma,a\sigma}(\omega)Z^R(\omega) \\ & \times[V^*_c g^R_c(\omega) + Mt_c V^*_a g^R_c(\omega)g^R_a(\omega)] \\ & + G^A_{d\sigma,a\sigma}(\omega)Z^R(\omega)[V^*_c g^<_c(\omega) + [g^R_c(\omega)g^<_a(\omega) \\ & + g^<_c(\omega)g^A_a(\omega)]\{Mt_c V^*_a + M|t_c|^2 Z^A(\omega)[V^*_c g^A_c \\ & + Mt_c V^*_a g^A_c(\omega)g^A_a(\omega)]\}. \end{aligned} \tag{A9}$$

Using Eqs. (A8) and (A9), we can express the steady current in Eq. (9) with the nonequilibrium Green's functions of the impurity. For simplicity, we will consider a flat density of states for the tip and host conduction electrons in the wide band limit given by

$$g^{R/A}_{a(c)}(\omega) = \mp i\pi\rho_{a(c)}, \tag{A10}$$

$$g^<_{a(c)}(\omega) = 2\pi i\rho_{a(c)}f_{a(c)}(\omega), \tag{A11}$$

where $\rho_{a(c)}$ is the density of states for noninteracting tip (host) conduction electrons at the Fermi level, and $f_{a(c)}(\omega)$ is its Fermi-Dirac distribution function. From Eqs. (9), (A8), and (A9) we obtain

$$\begin{aligned} J_{t\to h} = {} & \frac{e}{\hbar}\sum_{\sigma\tau}\int\frac{d\omega}{2\pi}\Bigg\{\frac{T_0}{2}[f_a(\omega)-f_c(\omega)] + G^<_{d\sigma\tau,d\sigma\tau}(\omega)T_{ac1} \\ & + G^R_{d\sigma\tau,d\sigma\tau}(\omega)2T_{ac1}f_c(\omega) \\ & + G^R_{d\sigma\tau,d\sigma\tau}(\omega)T_{ac2}[f_a(\omega)-f_c(\omega)] + \text{H.c.}\Bigg\}, \end{aligned} \tag{A12}$$

where

$$T_0 = \frac{4\gamma}{(1+M\gamma)^2},$$

$$T_{ac1} = i\pi\rho_a\frac{|V_a + iV_c t_c\pi\rho_c|^2}{(1+M\gamma)^2},$$

$$T_{ac2} = 2i\pi\rho_a\frac{(1-M\gamma)(V_a - iV_c t_c\pi\rho_c)^2}{(1+M\gamma)^3}.$$

Here $\gamma=\pi^2|t_c|^2\rho_a\rho_c$ is a measure of the strength for the direct tunneling of conduction electrons between the tip and host.

In a similar way we can find a current flowing from the host to the tip based on Eq. (10),

$$\begin{aligned} J_{h\to t} = {} & \frac{e}{\hbar}\sum_{\sigma\tau}\int\frac{d\omega}{2\pi}\Bigg\{\frac{T_0}{2}[f_c(\omega)-f_a(\omega)] + G^<_{d\sigma\tau,d\sigma\tau}(\omega)T_{ca1} \\ & + G^R_{d\sigma\tau,d\sigma\tau}(\omega)2T_{ca1}f_a(\omega) + G^R_{d\sigma\tau,d\sigma\tau}(\omega)T_{ca2}[f_c(\omega) \\ & - f_a(\omega)] + \text{H.c.}\Bigg\} + \frac{e}{\hbar}\frac{(M-1)\gamma}{1+M\gamma}\sum_{\sigma\tau}\int\frac{d\omega}{2\pi}\{G^<_{d\sigma\tau,d\sigma\tau}(\omega) \\ & \times(\Delta T_c + \Delta T_a) + 2G^R_{d\sigma\tau,d\sigma\tau}(\omega)\{\Delta T_c f_c(\omega) + \Delta T_a f_a(\omega) \\ & + \Delta T[f_c(\omega)-f_a(\omega)]\} + \text{H.c.}\}, \end{aligned} \tag{A13}$$

where

$$\Delta T_a = i\Gamma_a\frac{1}{1+M\gamma},$$

$$\Delta T_c = i\Gamma_c\left(1+\frac{1}{1+M\gamma}\right),$$

$$\Delta T = 2i\Gamma_c\frac{1}{(1+M\gamma)^2} + i\Gamma_a\frac{M\gamma-1}{(1+M\gamma)^2}.$$

T_{ca1} and T_{ca2} are just T_{ac1} and T_{ac2}, changing indices $a\leftrightarrow c$ while the hopping t_c is unchanged.

One can notice that the first term of the current $J_{h\to t}$ in Eq. (A13) is just the current $J_{t\to h}$ in Eq. (A12) if the tip and host are interchanged with each other. In the single-channel case $(M=1)$ the second term of the current $J_{h\to t}$ in Eq. (A13) vanishes; thus, the current formula satisfies the symmetry between the tip and host. However, in the multichannel case $(M>1)$ the symmetry is broken, because host conduction electrons are multichannel, whereas tip-conduction electrons are single channel.

APPENDIX B: SOLUTION FOR NCA EQUATIONS

In Appendix B we derive the NCA solution Eq. (43) with Eq. (44) and Eqs. (48) and (49) from Eqs. (41) and (42) and Eqs. (46) and (47), respectively. Introducing inverse Green's functions,[26,27]

$$Y_f(\omega) = -[G^R_f(\omega)]^{-1}, \tag{B1}$$

$$Y_b(\omega) = -[G^R_b(\omega)]^{-1}, \tag{B2}$$

one can rewrite Eqs. (41) and (42) as

$$\frac{dY_f(\omega)}{d\omega} = -1 - \frac{M\Gamma_c}{\pi}Y_b^{-1}(\omega), \tag{B3}$$

$$\frac{dY_b(\omega)}{d\omega} = -1 - \frac{N\Gamma_c}{\pi}Y_f^{-1}(\omega). \tag{B4}$$

Then, we find the exact relation between $Y_f(\omega)$ and $Y_b(\omega)$,

$$\frac{\pi}{M\Gamma_c}Y_b\exp\left(\frac{\pi}{M\Gamma_c}Y_b\right) = \left(\frac{Y_f}{T_K}\right)^{N/M}\exp\left(\frac{\pi}{M\Gamma_c}Y_f\right), \tag{B5}$$

where $T_K=D[M\Gamma_c/\pi D]^{M/N}\exp[\pi\varepsilon_d/N\Gamma_c]$ is the Kondo energy scale.

Solving Eq. (B5), we obtain

$$Y_b = \frac{M\Gamma_c}{\pi} W\left[\left(\frac{Y_f}{T_K}\right)^{N/M} \exp\left(\frac{\pi T_K}{M\Gamma_c}\frac{Y_f}{T_K}\right)\right], \tag{B6}$$

where $W[x]$ is the Lambert W function given by $x = W[x]\exp(W[x])$.[28] Inserting Y_b in Eq. (B6) into Eq. (B3), we find the solution given by Eq. (43) with Eq. (44).

Although NCA equations (46) and (47) for lesser self-energies are identical to differential equations (41) and (42) of retarded self-energies, Dyson equations (38) and (39) for the lesser Green's functions have a different structure. Together with Dyson equations (38) and (39), Eqs. (46) and (47) can be rewritten as

$$\frac{d[F^<(\omega)Y_f^2(\omega)]}{d\omega} = \frac{M\Gamma_c}{\pi} B^<(\omega), \tag{B7}$$

$$\frac{d[B^<(\omega)Y_b^2(\omega)]}{d\omega} = \frac{N\Gamma_c}{\pi} F^<(\omega) \tag{B8}$$

for frequency below E_0. Then, we find Eqs. (48) and (49) as their solution.

APPENDIX C: EFFECTIVE CHANNEL COUPLINGS

In this appendix we calculate the hybridization coupling of the channel $\tau=1$ $\Gamma^{c(1)}$ for the effective action of Eq. (57). We start from the following matrix identity:

$$(\mathbf{R} + x\mathbf{U})^{-1} = \mathbf{R}^{-1} - \frac{x}{1+xS}\mathbf{F}, \tag{C1}$$

where $\mathbf{R}_{ij}=R_i\delta_{ij}$ is a diagonal matrix, $\mathbf{U}_{ij}=1$ for all i and j, x is a number, $S=\Sigma_i R_i^{-1}$, and $\mathbf{F}_{ij}=R_i^{-1}R_j^{-1}$. Taking $\mathbf{R}=\delta_{kk'}(\omega-\varepsilon_k)$ and $x=-M|t_c|^2 g_a(\omega)$, we find the inversion of $[g_{kk'}^{c(1)}(\omega)]^{-1}$,

$$g_{kk'}^{c(1)}(\omega) = \frac{\delta_{kk'}}{\omega-\varepsilon_k} + \frac{M|t_c|^2 g_a(\omega)}{1-M|t_c|^2 g_a(\omega)g_c(\omega)} \frac{1}{\omega-\varepsilon_k}\frac{1}{\omega-\varepsilon_{k'}}, \tag{C2}$$

where $g_c(\omega)=\Sigma_{\mathbf{k}} 1/(\omega-\varepsilon_k)$. Performing the summation of $\mathbf{k}$, $\mathbf{k}'$ we obtain

$$\sum_{\mathbf{k}\mathbf{k}'} g_{kk'}^{c(1)}(\omega) = g_c(\omega) + \frac{M|t_c|^2 g_a(\omega)}{1-M|t_c|^2 g_a(\omega)g_c(\omega)}[g_c(\omega)]^2 = \frac{g_c(\omega)}{1-M|t_c|^2 g_a(\omega)g_c(\omega)}. \tag{C3}$$

In the wide band limit of a constant density of states for conduction electrons in both the host and tip, Eq. (C3) results in

$$\Gamma^{c(1)} = \frac{\Gamma_c}{1+M\gamma}. \tag{C4}$$

It also shows $\Gamma^{c(1)} \le \Gamma_c$.

We prove the identity Eq. (C1). Consider

$$(\mathbf{R}+x\mathbf{U})^{-1} = \sum_{n=0}^{\infty} (-1)^n x^n (\mathbf{R}^{-1}\mathbf{U})^n \mathbf{R}^{-1}. \tag{C5}$$

We introduce the following identity:

$$\sum_{n=1}^{\infty} (-1)^n x^n (\mathbf{R}^{-1}\mathbf{U})^n \mathbf{R}^{-1} = -x\left[\sum_{n=0}^{\infty} (-1)^n x^n (\mathbf{R}^{-1}\mathbf{U})^{n+1}\mathbf{R}^{-1}\right]. \tag{C6}$$

Since the matrix $\mathbf{R}$ is diagonal, we can write its inverse as $(\mathbf{R}^{-1})_{ij}=\tilde{R}_i\delta_{ij}$, where $\tilde{R}_i=1/R_i$. Calling $(\mathbf{R}^{-1}\mathbf{U})_{ij}=\tilde{R}_i$, where elements in each row are identical, we find

$$[(\mathbf{R}^{-1}\mathbf{U})^n]_{ij} = \tilde{R}_i S^{n-1} \tag{C7}$$

with $S=\Sigma_i \tilde{R}_i$. Inserting Eq. (C7) into Eq. (C6), we obtain

$$\sum_{n=1}^{\infty} (-1)^n x^n (\mathbf{R}^{-1}\mathbf{U})^n \mathbf{R}^{-1} = -x\left[\sum_{n=0}^{\infty} (-1)^n x^n S^n \mathbf{F}\right] = -\frac{x}{1+xS}\mathbf{F}, \tag{C8}$$

where $\mathbf{F}_{ij}=\tilde{R}_i\tilde{R}_j$. Resorting to Eqs. (C5) and (C8), finally, we reach Eq. (C1).

[1] V. Madhavan, W. Chen, T. Jamneala, M. F. Crommie, and N. S. Wingreen, Science **280**, 567 (1998).
[2] J. Li, W.-D. Schneider, R. Berndt, and B. Delley, Phys. Rev. Lett. **80**, 2893 (1998).
[3] H. C. Manoharan, C. P. Lutz, and D. M. Eigler, Nature (London) **403**, 512 (2000).
[4] U. Fano, Phys. Rev. **124**, 1866 (1961).
[5] O. Ujsaghy, J. Kroha, L. Szunyogh, and A. Zawadowski, Phys. Rev. Lett. **85**, 2557 (2000).
[6] A. Schiller and S. Hershfield, Phys. Rev. B **61**, 9036 (2000).
[7] M. Plihal and J. W. Gadzuk, Phys. Rev. B **63**, 085404 (2001).
[8] J. Gores, D. Goldhaber-Gordon, S. Heemeyer, M. A. Kastner, H. Shtrikman, D. Mahalu, and U. Meirav, Phys. Rev. B **62**, 2188 (2000).
[9] W. Hofstetter, J. Konig, and H. Schoeller, Phys. Rev. Lett. **87**, 156803 (2001).
[10] P. Nozieres and A. Blandin, J. Phys. (Paris) **41**, 193 (1980).
[11] Y. Oreg and D. Goldhaber-Gordon, Phys. Rev. Lett. **90**, 136602 (2003).
[12] C. L. Seaman, M. B. Maple, B. W. Lee, S. Ghamaty, M. S. Torikachvili, J. S. Kang, L. Z. Liu, J. W. Allen, and D. L. Cox, Phys. Rev. Lett. **67**, 2882 (1991).

[13] D. C. Ralph and R. A. Buhrman, Phys. Rev. Lett. **69**, 2118 (1992).
[14] D. L. Cox and A. Zawadowski, Adv. Phys. **47**, 599 (1998).
[15] I. Affleck and A. W. W. Ludwig, Phys. Rev. B **48**, 7297 (1993).
[16] D. L. Cox and A. E. Ruckenstein, Phys. Rev. Lett. **71**, 1613 (1993).
[17] O. Parcollet, A. Georges, G. Kotliar, and A. Sengupta, Phys. Rev. B **58**, 3794 (1998).
[18] L. V. Keldysh, Sov. Phys. JETP **20**, 1018 (1965).
[19] Y. Meir and N. S. Wingreen, Phys. Rev. Lett. **68**, 2512 (1992).
[20] N. S. Wingreen and Y. Meir, Phys. Rev. B **49**, 11040 (1994).
[21] M. H. Hettler, J. Kroha, and S. Hershfield, Phys. Rev. B **58**, 5649 (1998).
[22] D. C. Langreth, in *Linear and Nonlinear Electron Transport in Solids*, NATO Advanced Studies Institute, Series B: Physics, Vol. 17, edited by J. T. Devreese and V. E. Van Daren (Plenum, New York, 1976).
[23] H. Haug and A.-P. Jauho, *Quantum Kinetics in Transport and Optics of Semiconductors*, Series in Solid-State Sciences (Springer, Berlin, 1986).
[24] R. Landauer, IBM J. Res. Dev. **1**, 233 (1957); Philos. Mag. **21**, 863 (1970).
[25] M. Büttiker, Phys. Rev. Lett. **57**, 1761 (1986).
[26] E. Müller-Hartmann, Z. Phys. B **57**, 281 (1984).
[27] N. E. Bickers, Rev. Mod. Phys. **59**, 845 (1987).
[28] R. M. Corless, G. H. Gonnet, D. E. G. Hare, D. J. Jeffrey, and D. E. Knuth, Adv. Comput. Math. **5**, 329 (1996).
[29] *Handbook of Mathematical Functions with Formulas, Graphs, and Mathematical Tables*, edited by M. Abramowitz and I. A. Stegun (Dover Publications, New York, 1964).
[30] K. Yosida and K. Yamada, Prog. Theor. Phys. Suppl. **46**, 244 (1970); K. Yamada, Prog. Theor. Phys. **53**, 970 (1975); K. Yosida and K. Yamada, *ibid.* **53**, 1286 (1975); K. Yamada, *ibid.* **54**, 316 (1975).
[31] C. M. Varma, P. B. Littlewood, S. Schmitt-Rink, E. Abrahams, and A. E. Ruckenstein, Phys. Rev. Lett. **63**, 1996 (1989).
[32] P. Gegenwart, Q. Si, and F. Steglich, Nat. Phys. **4**, 186 (2008); H. v. Löhneysen, A. Rosch, M. Vojta, and P. Wolfle, Rev. Mod. Phys. **79**, 1015 (2007).
[33] J. Rech, P. Coleman, G. Zarand, and O. Parcollet, Phys. Rev. Lett. **96**, 016601 (2006).